Supporting Information

Nitrogen-doping to accelerate phase transition to ordered intermetallic Pt_3Co catalyst for oxygen reduction reaction in fuel cells

Weicheng Xu [a], Zhipeng Zhu [a], Yucheng Wang *[ab], Peixin Cui [c], Lei Tong [d], Kuangmin Zhao [a], Jiayin Yuan [e], Zhi-You Zhou [ab], Hai-Wei Liang *[d], Na Tian *[a] and Shi-Gang Sun *[a]

[a] State Key Laboratory of Physical Chemistry of Solid Surfaces, Collaborative Innovation Center of Chemistry for Energy Materials, College of Chemistry and Chemical Engineering, Xiamen University, Xiamen 361005, China

[b] Innovation Laboratory for Sciences and Technologies of Energy Materials of Fujian Province (IKKEM) Xiamen 361005, China

[c] Key Laboratory of Soil Environment and Pollution Remediation, Institute of Soil Science, Chinese Academy of Sciences, Nanjing 210008, China

[d] Hefei National Laboratory for Physical Sciences at the Microscale, Department of Chemistry, University of Science and Technology of China, Hefei 230026, China

[e] Department of Materials and Environmental Chemistry, Stockholm University, Stockholm 10691, Sweden

* Corresponding authors. E-mail: wangyc@xmu.edu.cn, hwliang@ustc.edu.cn, tnsd@xmu.edu.cn, sgsun@xmu.edu.cn

Supporting Figures and Tables

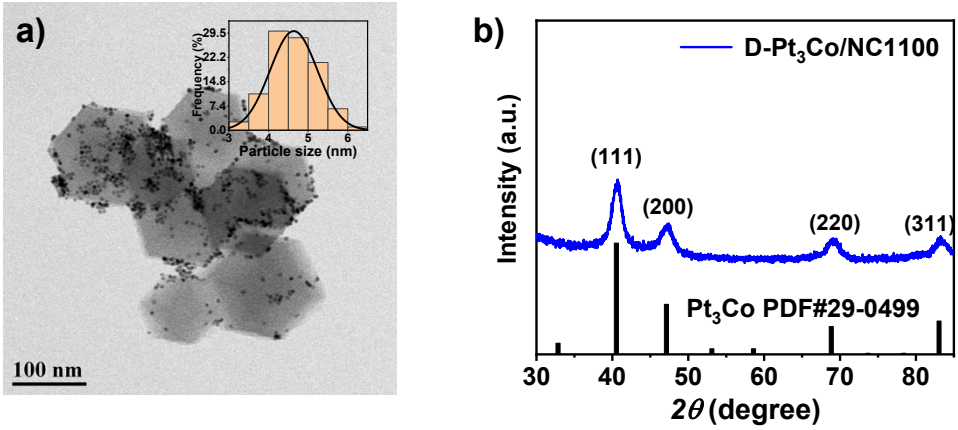

Fig. S1. (a) TEM image of D-Pt_3Co/NC1100, the inset shows the particle size statistics of more than 200 particles. (b) XRD pattern of D-Pt_3Co/NC1100.

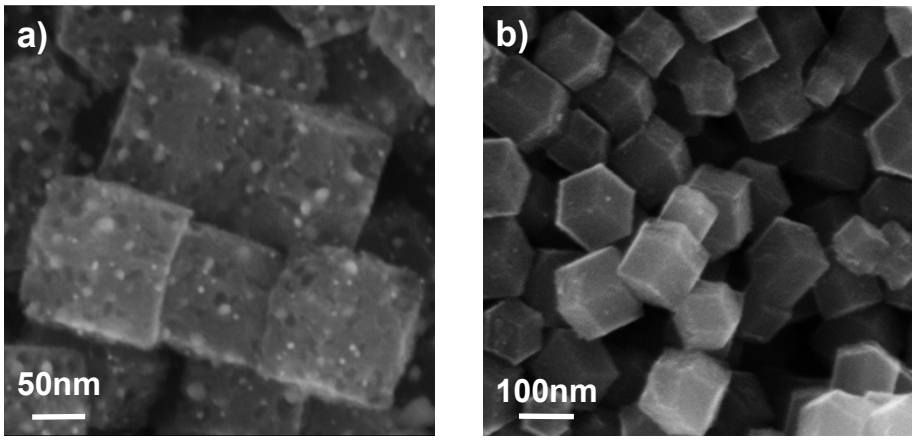

Fig. S2. (a) SEM images of O-Pt_3Co/NC1100 and (b) NC1100.

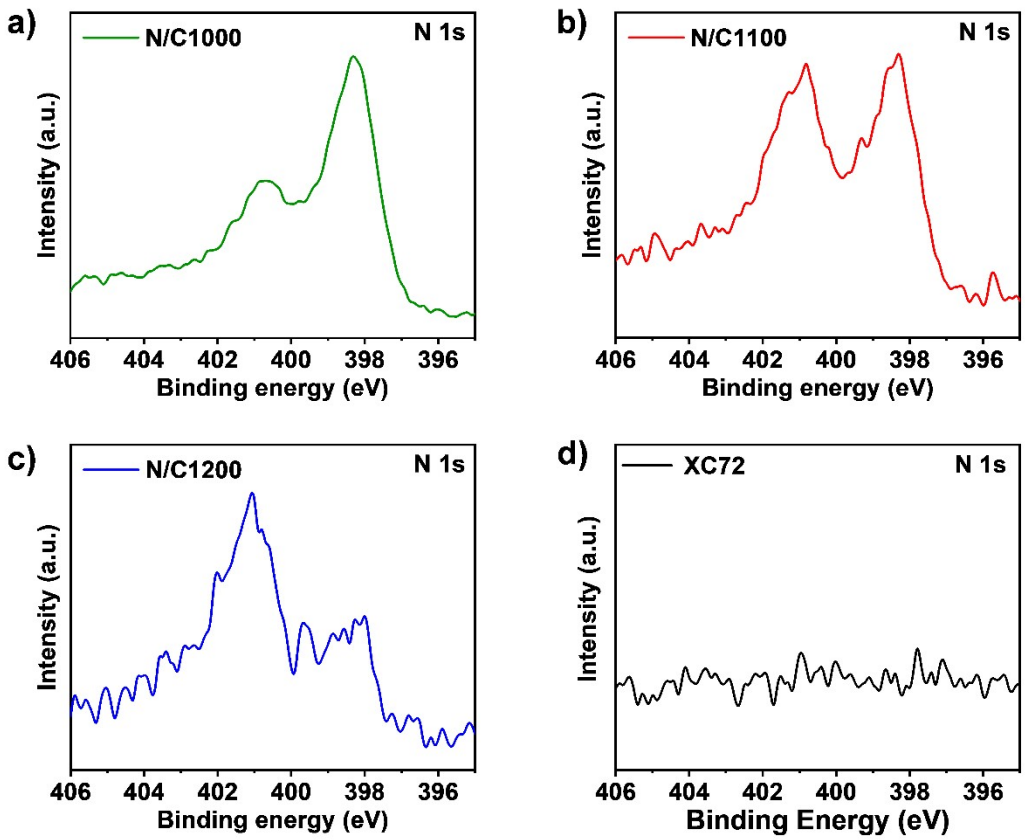

Fig. S3. High resolution N 1*s* XPS spectra of (a) NC1000, (b) NC1100, (c) NC1200, and (d) XC72.

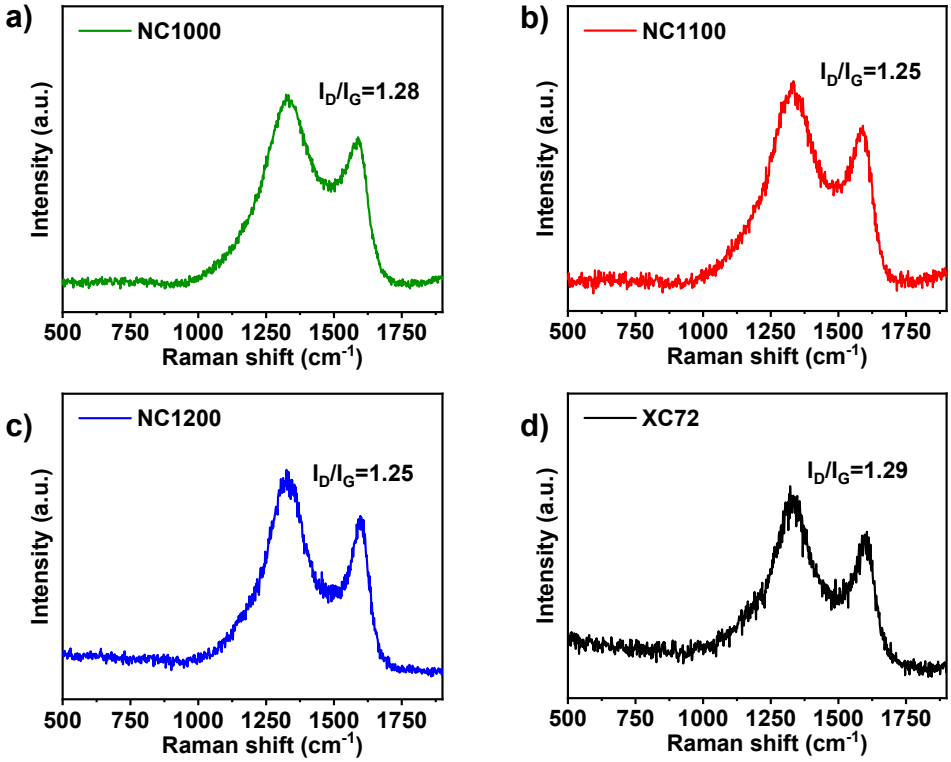

Fig. S4. Raman spectra of (a) NC1000, (b) NC1100, (c) NC1200 and (d) XC72. The value of I_D/I_G can represent the graphitization degree of carbon support, the I_D/I_G value of the four carbon supports was basically the same, indicating a similar graphitization degree.

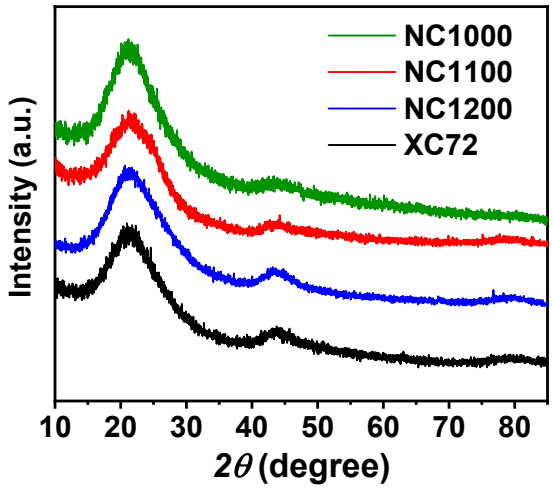

Fig. S5. XRD patterns of NC1000, NC1100, NC1200 and XC72.

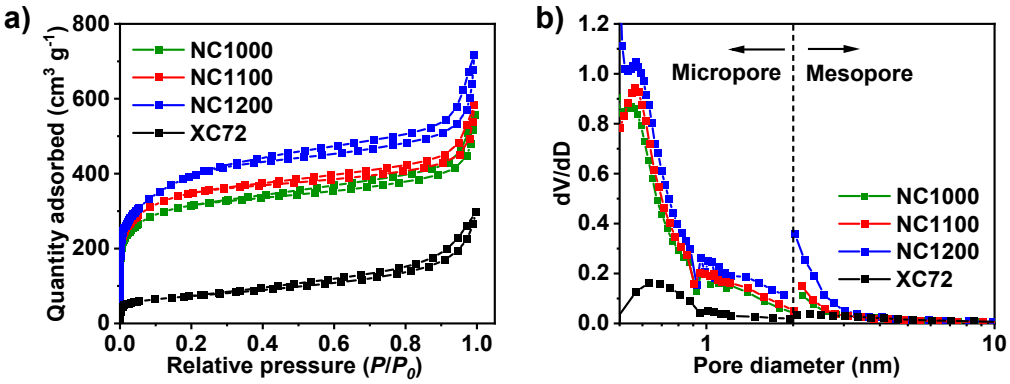

Fig. S6. (a) N_2 adsorption/desorption isotherms of NC1000, NC1100, NC1200 and XC72. (b) Pore size distribution curves calculated by BJH (mesopore) and HK method (Micropore).

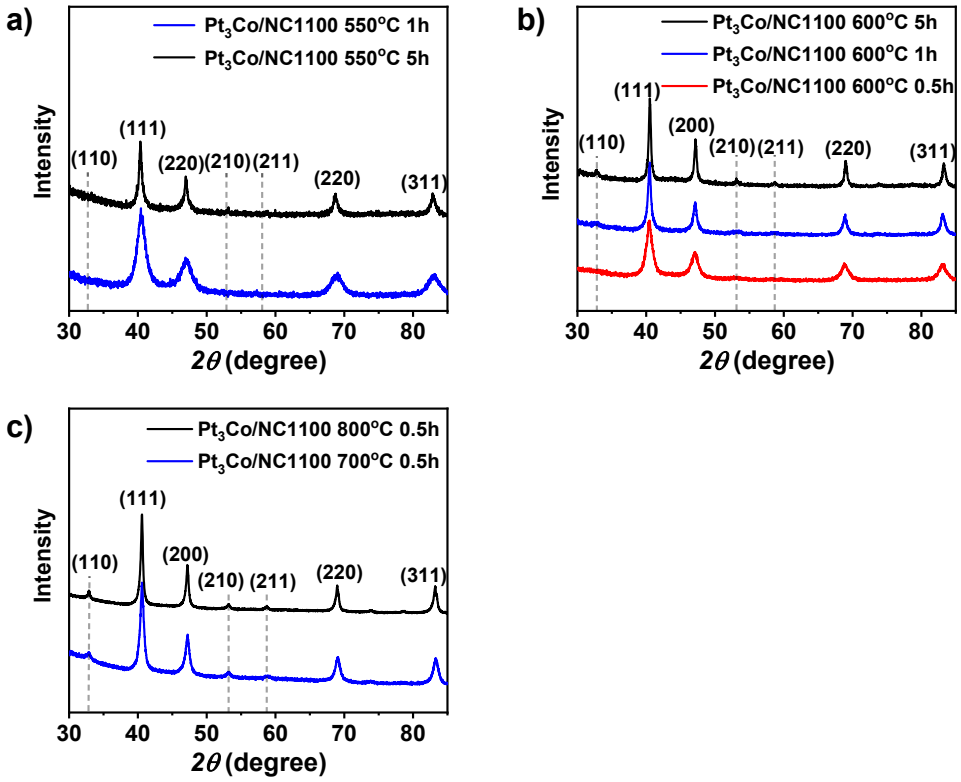

Fig. S7. XRD patterns of Pt_3Co/NC1100 annealed at (a) 550℃ 1h, 5h. (b) 600℃ 0.5h, 1h, 5h. (c) 700℃ 0.5h, 800℃ 0.5h.

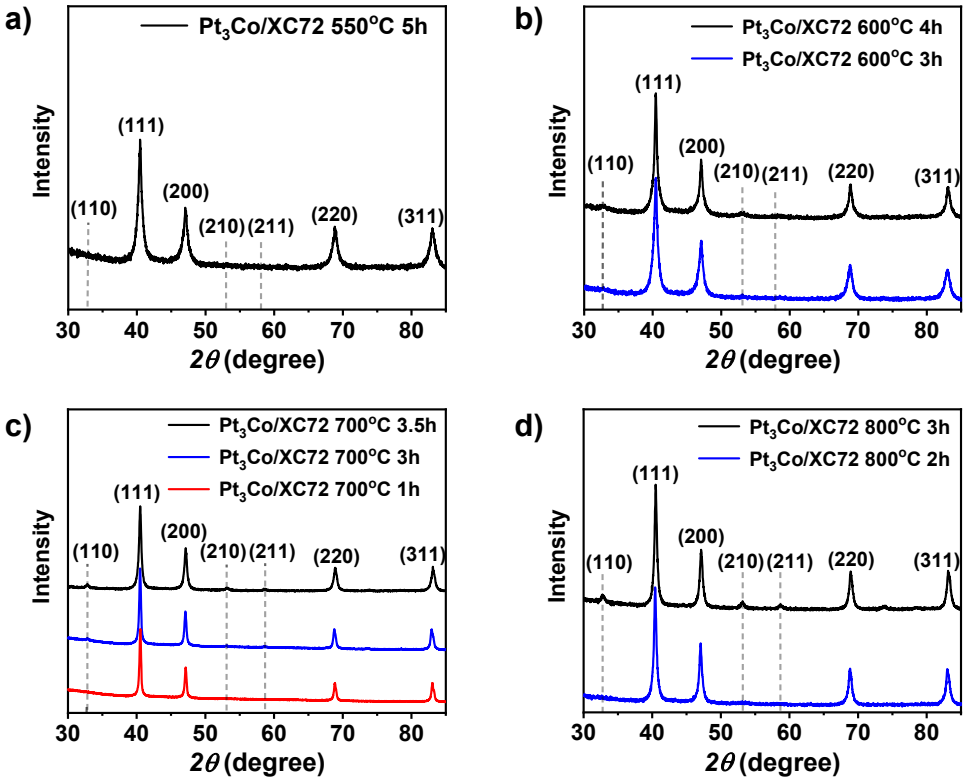

Fig. S8. XRD patterns of Pt_3Co/XC72 annealed at (a) 550°C 5h. (b) 600°C 3h, 4h. (c) 700°C, 1h, 3h, 3.5h. (d) 800°C, 2h, 3h.

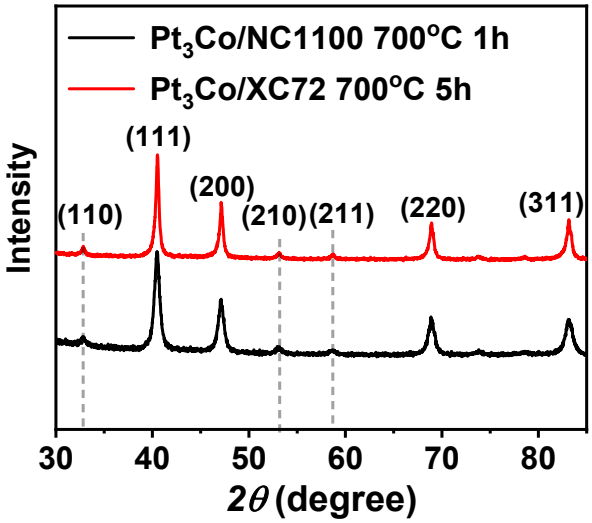

Fig. S9. XRD patterns of Pt_3Co/NC1100 annealed at 700 °C for 1 h, Pt_3Co/XC72 annealing at 700 °C for 5 h.

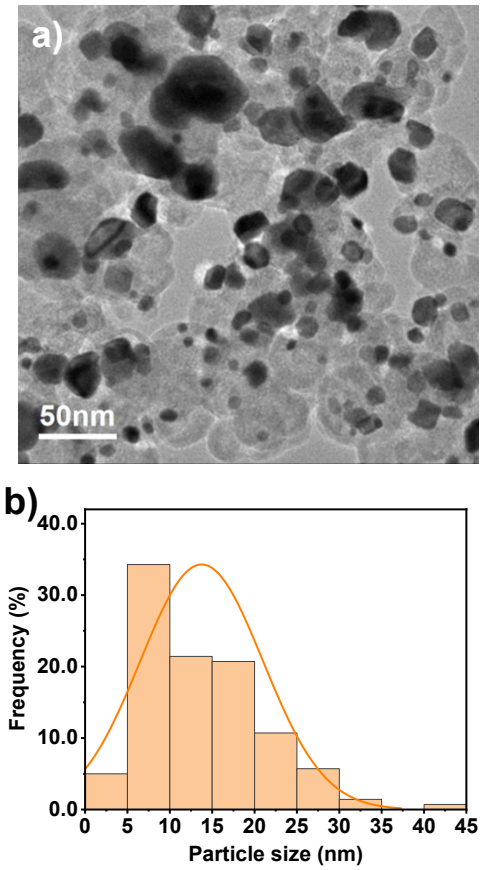

Fig. S10. (a) TEM image of O-Pt_3Co/XC72 annealed at 700°C for 5h. (b) Particle size histrogram of more than 150 particles.

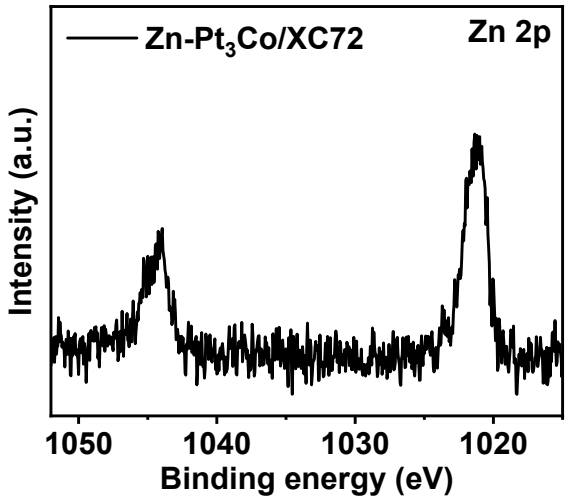

Fig. S11. High-resolution Zn 2*p* XPS of Zn-Pt_3Co/XC72.

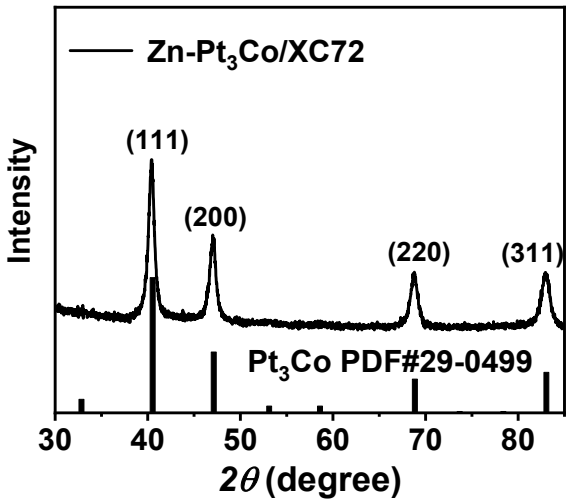

Fig. S12. XRD patterns of Zn-Pt_3Co/XC72 synthesized in the same way as O-Pt_3Co/NC1100 with only the change of the support and the addition of trace zinc chloride.

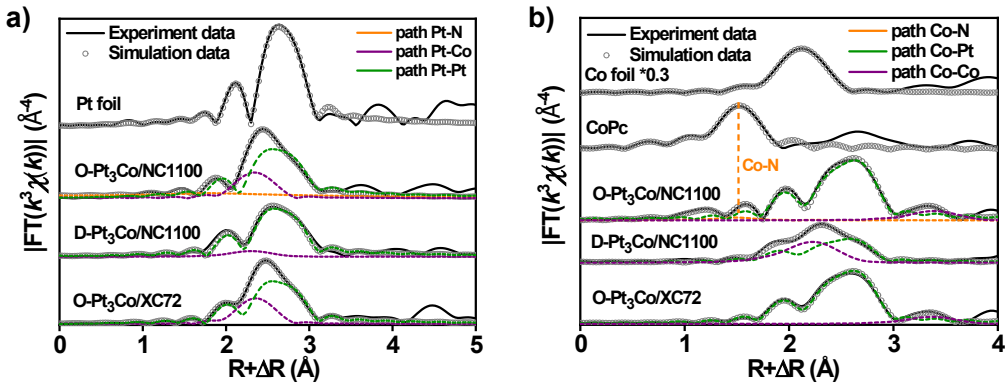

Fig. S13. (a) Pt EXAFS fitting in R space for D-Pt_3Co/NC1100, O-Pt_3Co/NC1100, O-Pt_3Co/XC72 and Pt foil. (b) Co EXAFS fitting in R space for D-Pt_3Co/NC1100, O-Pt_3Co/NC1100, O-Pt_3Co/XC72, CoPc and Co foil.

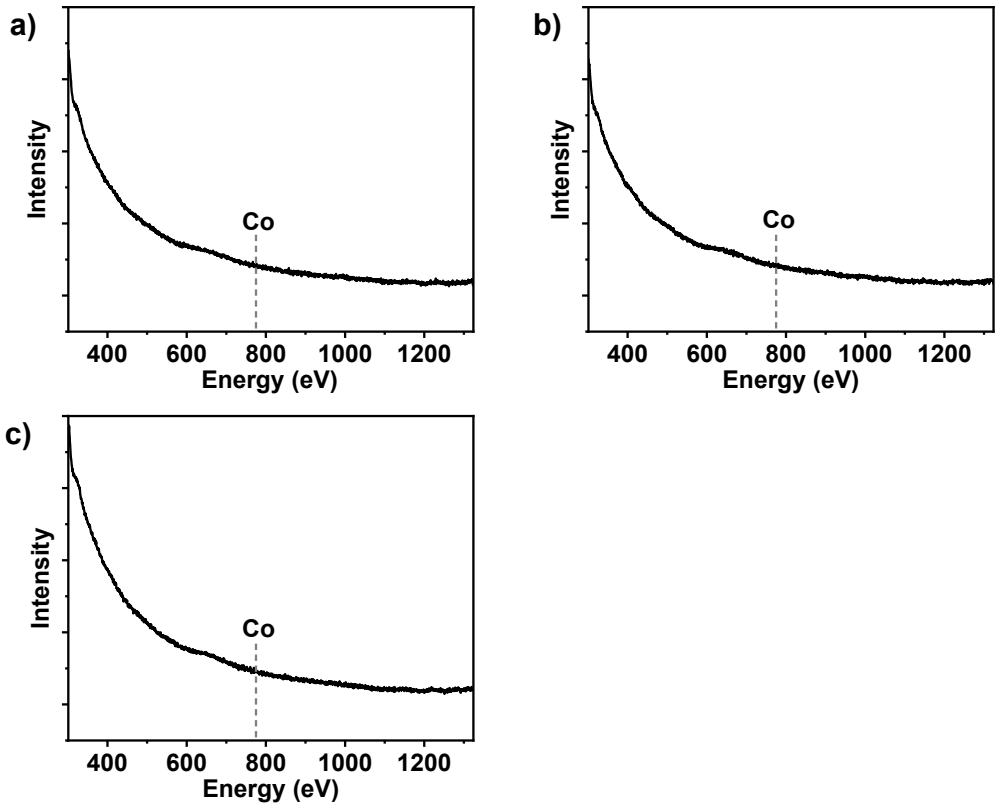

Fig. S14. EELS analysis of the Co elemental composition in three different regions free of alloy particles.

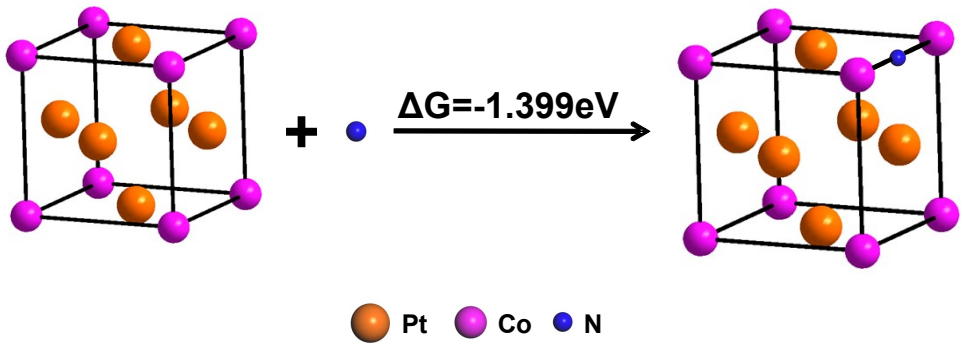

Fig. S15. Calculation of thermodynamic free energy variation after N doping at 25 ℃ and standard atmospheric pressure.

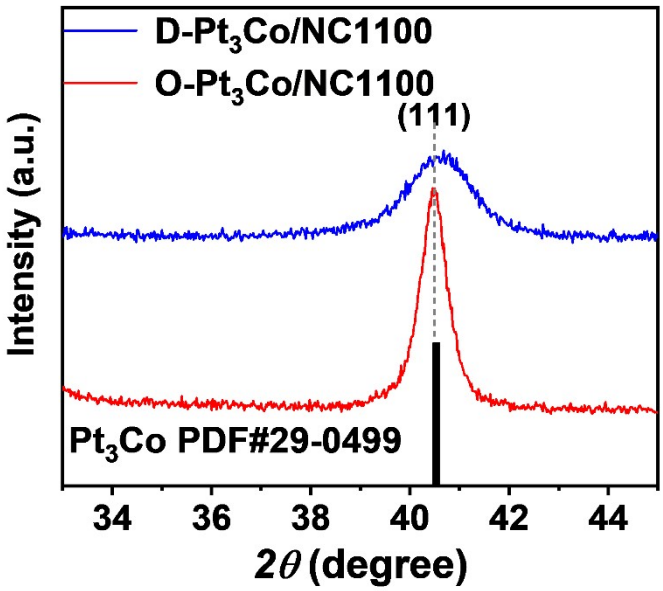

Fig. S16 Comparison of (111) XRD diffraction peak between O-Pt_3Co/NC1100 and D-Pt_3Co/NC1100. The slight negative shift (0.14°) in (111) diffraction peak of O-Pt_3Co/NC1100 indicates the lattice expansion, which may be induced by N doping into the lattice interstitial position of Pt_3Co.

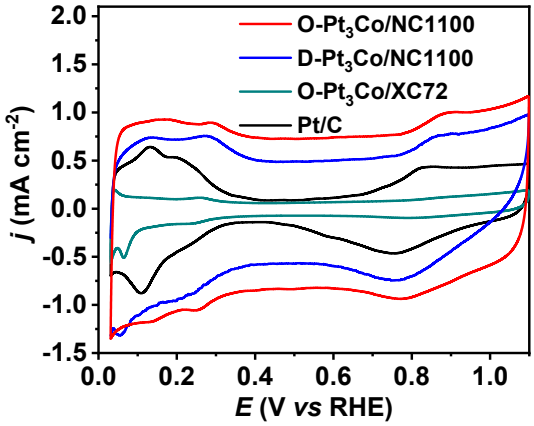

Fig. S17. Cyclic voltammetric curves of O-Pt_3Co/NC1100, D-Pt_3Co/NC1100, O-Pt_3Co/XC72, and commercial Pt/C in an Ar-saturated 0.1 M $HClO_4$ solution.

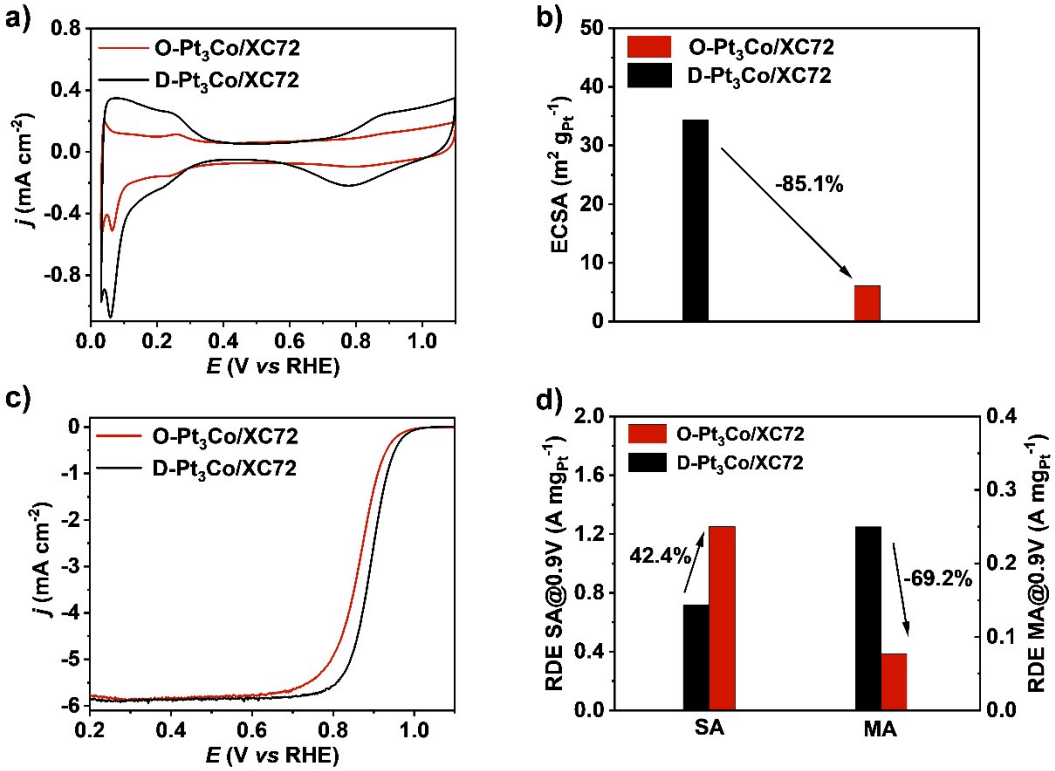

Fig. S18. (a) Cyclic voltammograms of O-Pt_3Co/XC72 and D-Pt_3Co/XC72 in Ar-saturated 0.1 M $HClO_4$ solution. (b) Comparison of ECSA between O-Pt_3Co/XC72 and D-Pt_3Co/XC72. (c) ORR polarization curves of O-Pt_3Co/XC72 and D-Pt_3Co/ XC72 in O_2-saturated 0.1 M $HClO_4$ solution. (d) Specific activity and mass activity of O-Pt_3Co/XC72 and D-Pt_3Co/XC72 at 0.90 V *vs*. RHE.

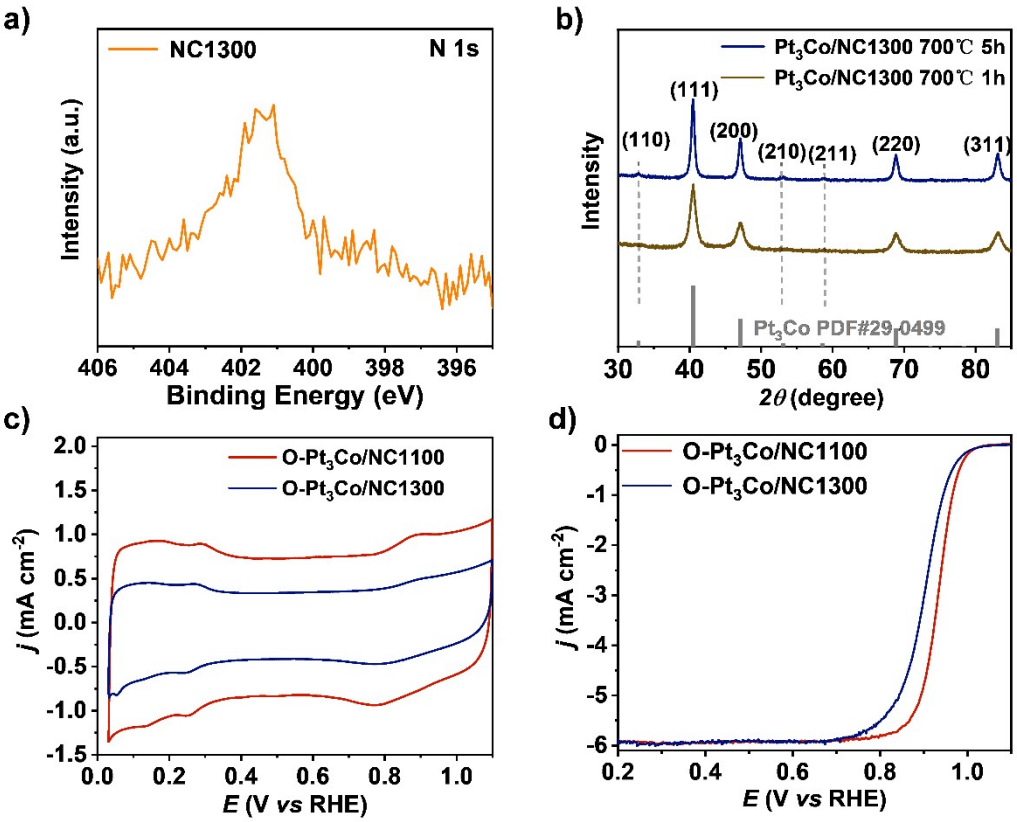

Fig. S19. (a) High resolution N 1*s* XPS of NC1300. (b) XRD patterns of Pt_3Co/NC1300 annealed at 700 °C for 1 and 5 h. (c) Cyclic voltammograms of O-Pt_3Co/NC1100 and O-Pt_3Co/NC1300 in Ar-saturated 0.1 M $HClO_4$ solution. (d) ORR polarization curves of O-Pt_3Co/NC1100 and O-Pt_3Co/NC1300 in O_2-saturated 0.1 M $HClO_4$ solution.

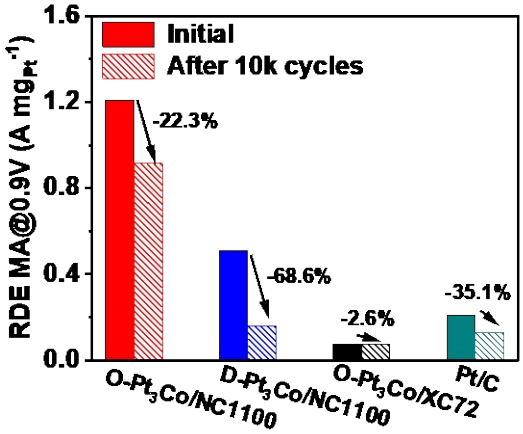

Fig. S20. Mass activity of O-Pt_3Co/NC1100, D-Pt_3Co/NC1100, O-Pt_3Co/XC72 and Pt/C at 0.9 V *vs.* RHE before and after ADT tests.

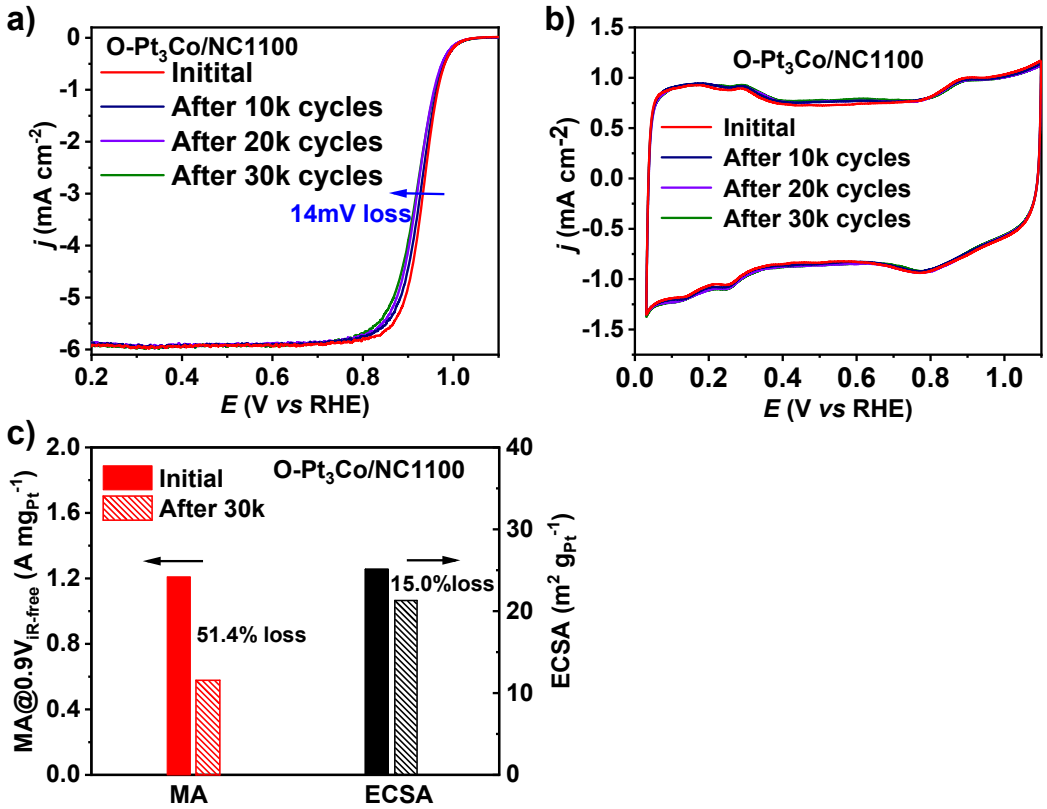

Fig. S21. (a) ORR polarization curves of O-Pt_3Co/NC1100 before and after ADT. (b) Cyclic voltammograms of O-Pt_3Co/NC1100 before and after ADT. (c) Mass activity and ECSA of O-Pt_3Co/NC1100 at 0.9 V *vs.* RHE before and after ADT.

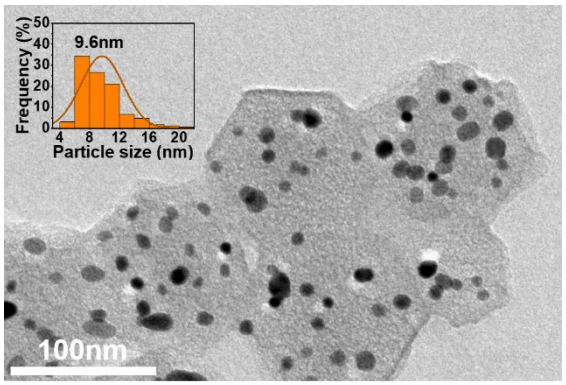

Fig. S22. TEM image of O-Pt_3Co/NC1100 after ADT on fuel cell. The inset shows the size histogram.

Table S1. Contents of N, Co, Pt element in NC1000, NC1100, NC1200, NC1300, XC72, O-Pt_3Co/NC1100, D-Pt_3Co/NC1100, O-Pt_3Co/XC72 and D-Pt_3Co/XC72 obtained by XPS analysis, and Pt (wt%) in O-Pt_3Co/NC1100, D-Pt_3Co/NC1100 and O-Pt_3Co/XC72 obtained by ICP-OES.

	N (at%)	Zn (at%)	Co (at%)	Pt (at%)	Pt (wt%)
N/C1000	9.86	1.99	\	\	\
N/C1100	4.64	0.74	\	\	\
N/C1200	2.52	0.22	\	\	\
N/C1300	1.42	0.10	\	\	\
XC72	\	\	\	\	\
O-Pt_3Co/NC1100	2.92	0.43	0.19	0.54	12.5
D-Pt_3Co/NC1100	3.16	0.37	0.65	3.43	12.0
O-Pt_3Co/XC72	\	\	0.34	0.87	15.1
D-Pt_3Co/XC72	\	\	0.47	1.73	--

Table S2. Comparison of intensity ratio of (110)/(111) peaks, phase structure, and grain sizes of different catalysts according to the XRD data.

Catalyst	Intensity ratio of (110)/(111) peaks	Phase[a]	Grain size (nm)[b]
Pt_3Co/NC1000 700°C 1h	0.097	Order	11.6
Pt_3Co/NC1100 550°C 1h	N/A	Disorder	6.0
Pt_3Co/NC1100 550°C 5h	N/A	Disorder	10.3
Pt_3Co/NC1100 600°C 0.5h	0.021	Disorder	6.8
Pt_3Co/NC1100 600°C 1h	0.062	Order	8.2
Pt_3Co/NC1100 600°C 5h	0.081	Order	12.9
Pt_3Co/NC1100 700°C 0.5h	0.085	Order	8.9
Pt_3Co/NC1100 700°C 1h	0.098	Order	8.8
Pt_3Co/NC1100 800°C 0.5h	0.092	Order	12.8
Pt_3Co/NC1200 700°C 1h	N/A	Disorder	11.2
Pt_3Co/NC1300 700°C 1h	N/A	Disorder	6.9
Pt_3Co/NC1300 700°C 5h	0.061	Order	10.0
Pt_3Co/XC72 550°C 5h	N/A	Disorder	8.8
Pt_3Co/XC72 600°C 3h	0.015	Disorder	9.4
Pt_3Co/XC72 600°C 4h	0.051	Order	10.9
Pt_3Co/XC72 700°C 1h	N/A	Disorder	11.9
Pt_3Co/XC72 700°C 3h	0.015	Disorder	12.0
Pt_3Co/XC72 700°C 3.5h	0.053	Order	12.1
Pt_3Co/XC72 700°C 5h	0.091	Order	12.5
Pt_3Co/XC72 800°C 2h	N/A	Disorder	11.3
Pt_3Co/XC72 800°C 3h	0.068	Order	11.5

a: The catalyst is considered as an ordered alloy if the intensity ratio of (110)/(111) is greater than 0.05, considering that the ratio on the standard card (Pt_3Co PDF#29-0499) is 0.10.

b: The average grain sizes of Pt_3Co nanoparticles were obtained by calculating the half-peak width of (111) XRD peak using Scherrer's formula.

Table S3. Analysis of Pt 4*f* XPS peak including peak position, half peak width and integral area.

Component	Position (eV)		FWHM (eV)		Area	
	$4f_{5/2}$	$4f_{7/2}$	$4f_{5/2}$	$4f_{7/2}$	$4f_{5/2}$	$4f_{7/2}$
D-Pt_3Co/XC72 Pt^0	71.5	74.9	0.95	1.12	26095.6	26119.2
D-Pt_3Co/XC72 Pt^{2+}	72.3	76.0	0.90	1.20	4589.3	3481.5
O-Pt_3Co/XC72 Pt^0	71.5	74.8	0.85	1.06	2099.7	2080.6
O-Pt_3Co/XC72 Pt^{2+}	72.2	76.0	0.95	1.01	306.9	171.6
D-Pt_3Co/NC1100 Pt^0	71.3	74.6	0.90	1.08	19269.4	18404.1
D-Pt_3Co/NC1100 Pt^{2+}	72.2	75.6	0.91	1.00	2474.6	2026.2
O-Pt_3Co/NC1100 Pt^0	71.3	74.5	0.78	1.00	5261.6	4922.3
O-Pt_3Co/NC1100 Pt^{2+}	72.1	75.5	0.71	1.00	537.4	495.3

The annealing condition is 700 ℃, 1 hour for O-Pt_3Co/NC1100; 700 ℃, 5 hour for O-Pt_3Co/XC72, D-Pt_3Co/NC1100 and D-Pt_3Co/XC72 are not annealed.

Table S4. Analysis of Co $2p_{3/2}$ XPS peak including peak position, half peak width and integral area

Component	Position (eV)	FWHM (eV)	Area
D-Pt_3Co/XC72 Co^0	778.6	1.81	4619.6
D-Pt_3Co/XC72 Co^{2+}	781.5	2.20	2900.1
O-Pt_3Co/XC72 Co^0	778.4	2.51	589.9
O-Pt_3Co/XC72 Co^{2+}	781.1	2.60	420.2
D-Pt_3Co/NC1100 Co^0	778.3	2.02	764.9
D-Pt_3Co/NC1100 Co^{2+}	781.2	2.03	497.9
O-Pt_3Co/NC1100 Co^0	778.2	3.01	1048.0
O-Pt_3Co/NC1100 Co^{2+}	780.4	2.90	1537.9

Table S5. EXAFS fitting parameters at the Pt L_3-edge for various samples（S_0^2=0.829）

	Shell	N^a	R(Å)^b	σ^2(Å^2)^c	E_0(eV)^d	R factor
Pt foil	Pt-Pt	12	2.76	0.0046	8.7	0.0016
O-Pt_3Co/NC1100	Pt-N	0.1	2.12	0.0109	6.6	0.0017
	Pt-Co	3.0	2.69	0.0069		
	Pt-Pt	8.6	2.71	0.0065		
O-Pt_3Co/XC72	Pt-Co	2.7	2.69	0.0072	7.7	0.0002
	Pt-Pt	8.2	2.73	0.0063		
D-Pt_3Co/NC1100	Pt-Co	1.3	2.65	0.0121	6.9	0.0066
	Pt-Pt	9.1	2.74	0.0055		

$^a N$: coordination numbers; $^b R$: bond distance; $^c \sigma^2$: Debye-Waller factors; $^d \Delta E_0$: the inner potential correction. R factor: goodness of fit. S_0^2 was set to 0.829, according to the experimental EXAFS fit of Pt foil reference by fixing CN as the known crystallographic value.

Table S6. EXAFS fitting parameters at the Co K-edge for various samples（S_0^2=0.749）

	Shell	N^a	R(Å)^b	σ^2(Å^2)^c	E_0(eV)^d	R factor
Co foil	Co-Co	12	2.50	0.0063	-6.0	0.0010
CoPc	Co-N	4.0	1.95	0.0015	4.2	0.0078
O-Pt_3Co/NC1100	Co-N	0.3	1.95	0.0018	-3.7	0.0063
	Co-Co	10.6	2.70	0.0066		
	Co-Pt	3.0	3.80	0.0088		
O-Pt_3Co/XC72	Co-Co	8.7	2.69	0.0050	-5.0	0.0077
	Co-Pt	2.7	3.79	0.0098		
D-Pt_3Co/NC1100	Co-Co	5.3	2.65	0.0079	-5.2	0.0008
	Co-Pt	4.3	2.62	0.0131		

$^a N$: coordination numbers; $^b R$: bond distance; $^c \sigma^2$: Debye-Waller factors; $^d \Delta E_0$: the inner potential correction. R factor: goodness of fit. S_0^2 was set to 0.749, according to the experimental EXAFS fit of Co foil reference by fixing CN as the known crystallographic value.

Table S7. H_2-air PEMFC performance and mass activity comparison with advanced Pt-based catalyst in recent five years.

Catalyst	Pt loading (mg_{Pt} cm^{-2})	Outlet Pressure (kPa)	Flow Rate (sccm)	Active Aera (cm^2)	Power Density@0.6V (W cm^{-2})	MA@0.9V (A mg_{Pt}^{-1})	Ref.
O-Pt_3Co/NC1100	0.05/0.1	150	600/2600	12.96	1.27	1.19	This work
Co doped Pt	0.025/0.2	250	300/800	6.25	~1.02	--	1
$L1_0$-W-PtCo/C	0.1/0.11	150	200/500	--	~0.6	0.57	2
LP@PF-2	0.35/0.035	150	200/780	5	0.78	1.77	3
$L1_0$-PtZn-C	0.1/0.104	150	500/1000	--	0.81	0.52	4
PtCo i-NPs	0.02/0.02	250	500/2000	5	1.08	1.52	5
Pt_3Co/FeN_4-C	~0.1/~0.1	150	500/1000	5	~0.92	0.72	6
P_{NS}-Pt/C	0.05/0.15	150	stoi. 2/2	25	~1.06	--	7
oh-PtNi(Mo)/C	0.1/0.1	100	stoi. 1.5/2	50	~0.82	--	8

1. X. Duan, F. Cao, R. Ding, X. Li, Q. Li, R. Aisha, S. Zhang, K. Hua, Z. Rui, Y. Wu, J. Li, A. Li and J. Liu, *Adv. Energy. Mater.*, 2022, **12**.
2. J. Liang, N. Li, Z. Zhao, L. Ma, X. Wang, S. Li, X. Liu, T. Wang, Y. Du, G. Lu, J. Han, Y. Huang, D. Su and Q. Li, *Angew. Chem. Int. Ed.*, 2019, **58**, 15471-15477.
3. L. Chong, J. G. Wen, J. Kubal, F. G. Sen, J. X. Zou, J. Greeley, M. Chan, H. Barkholtz, W. J. Ding and D. J. Liu, *Science*, 2018, **362**, 1276-+.
4. J. Liang, Z. Zhao, N. Li, X. Wang, S. Li, X. Liu, T. Wang, G. Lu, D. Wang, B. J. Hwang, Y. Huang, D. Su and Q. Li, *Adv. Energy. Mater.*, 2020, **10**.
5. C.-L. Yang, L.-N. Wang, P. Yin, J. Liu, M.-X. Chen, Q.-Q. Yan, Z.-S. Wang, S.-L. Xu, S.-Q. Chu, C. Cui, H. Ju, J. Zhu, Y. Lin, J. Shui and H.-W. Liang, *Science*, 2021, **374**, 459-464.

6. X. Li, Y. He, S. Cheng, B. Li, Y. Zeng, Z. Xie, Q. Meng, L. Ma, K. Kisslinger, X. Tong, S. Hwang, S. Yao, C. Li, Z. Qiao, C. Shan, Y. Zhu, J. Xie, G. Wang, G. Wu and D. Su, *Adv. Mater.*, 2021.
7. B.-A. Lu, L.-F. Shen, J. Liu, Q. Zhang, L.-Y. Wan, D. J. Morris, R.-X. Wang, Z.-Y. Zhou, G. Li, T. Sheng, L. Gu, P. Zhang, N. Tian and S.-G. Sun, *ACS Catal.*, 2021, **11**, 355-363.
8. F. Dionigi, C. C. Weber, M. Primbs, M. Gocyla, A. M. Bonastre, C. Spöri, H. Schmies, E. Hornberger, S. Kühl, J. Drnec, M. Heggen, J. Sharman, R. E. Dunin-Borkowski and P. Strasser, *Nano Letters*, 2019, **19**, 6876-6885.